Estimating constituent concentrations in case II waters from MERIS satellite data by semi-analytical model optimizing and look-up tables

Wei Yang[1,2], Bunkei Matsushita[2*], Jin Chen[1], Takehiko Fukushima[2]

[1] State key laboratory of earth surface processes and resource ecology, Beijing Normal University, Beijing, 100875, China

E-mail: yangwei1022@gmail.com, chenjin@ires.cn

[2]Graduate School of Life and Environmental Sciences, University of Tsukuba

1-1-1 Tennoudai, Tsukuba, Ibaraki, 305-8572, Japan

E-mails: mbunkei@sakura.cc.tsukuba.ac.jp,

fukusima@sakura.cc.tsukuba.ac.jp

Submittal date: 2010-9-17

*Corresponding Author

E-mail: mbunkei@sakura.cc.tsukuba.ac.jp

Estimating constituent concentrations in case II waters from MERIS satellite data by semi-analytical model optimizing and look-up tables

Abstract

Remote estimation of water constituent concentrations in case II waters has been a great challenge, primarily due to the complex interactions among the phytoplankton, tripton, colored dissolved organic matter (CDOM) and pure water. Semi-analytical algorithms for estimating constituent concentrations are effective and easy to implement, but two challenges remain. First, a dataset without a sampling bias is needed to calibrate estimation models; and second, the semi-analytical indices were developed based on several specific assumptions that may not be universally applicable. In this study, a semi-analytical model-optimizing and look-up-table (SAMO-LUT) method was proposed to address these two challenges. The SAMO-LUT method is based on three previous semi-analytical models to estimate chlorophyll *a*, tripton and CDOM. Look-up tables and an iterative searching strategy were used to obtain the most appropriate parameters in the models. Three datasets (i.e., noise-free simulation data, *in situ* data and MEdium Resolution Imaging Spectrometer (MERIS) satellite data) were collected to validate the performance of the proposed method. The results show that the SAMO-LUT method yields error-free results for the ideal simulation dataset; and is able also to accutrately estimate the water constituent concentrations with an average bias (mean normalized bias, MNB) lower than 9% and relative random uncertainty (normalized root mean square error, NRMS) lower than 34% even for *in situ* and MERIS data. These results demonstrate the potential of the proposed algorithm to accurately monitor

inland and coastal waters based on satellite observations.

Key words: semi-analytical models; look-up table; bio-optical model; case II water

1. Introduction

Accelerated eutrophication of inland water is becoming a significant environmental issue all over the world (Ayres et al., 1996). The sustainable management of freshwater ecosystems requires the routine monitoring of water quality. However, the spatial and temporal heterogeneity of water bodies coupled often result in inadequate monitoring and characterization of water quality using conventional sampling methods (Khorram et al., 1991; Liu et al., 2003). Consequently a combined approach utilizing the spatial and temporal coverage of remote sensing with conventional water sampling provides a potentially effective solution to monitoring freshwater ecosystems.

From the remote sensing perspective, aquatic environments can be classified as either case I or case II waters (Morel and Prieur, 1977). While case I waters are those dominated by phytoplankton (e.g. open ocean), case II waters contain tripton, dissolved organic matter in addition to phytoplankton. It has been shown that concentrations of total suspended solids (TSS) and organic matter are not necessarily correlated with chlorophyll *a* concentration in both coastal and inland case II waters (Gin et al., 2003; Nichol, 1993). The use of a remote sensing technique for water quality monitoring in case II waters has been far less successful compared with that in case I waters, due mainly to the complex interactions of the four optically active substances (OASs; i.e., phytoplankton,

64 tripton, colored dissolved organic matter (CDOM) and pure water) in case II waters (Doxaran et al.,
65 2002; Gin et al., 2002; Goodin et al., 1993).

66 To address the difficulties of monitoring case II waters, researchers have made substantial
67 efforts to accurately estimate water constituent concentrations (including concentrations of
68 chlorophyll *a* and tripton as well as absorption of CDOM at 440 nm). These efforts have included
69 the use of derivative values of reflectance spectra (Goodin et al., 1993), examination of the band
70 ratio of near infrared reflectance and red reflectance (Han et al., 1994), use of the inherent optical
71 property (IOP) inversion technique based on a bio-optical model (Brando and Dekker, 2003; Garver
72 and Siegel, 1997; Santini et al., 2010) or on the use of Hydrolight (Mobley et al., 2005; Van Der
73 Woerd and Pasterkamp, 2008), and use of the spectral mixture analysis technique to minimize the
74 interactions of the four OASs (Novo et al., 2006; Oyama et al., 2009; Oyama et al., 2007; Svab et al.,
75 2005; Tyler et al., 2006).

76 Additionally, several semi-analytical algorithms have been proposed to estimate water
77 constituent concentrations in case II waters (e.g., Ammenberg et al., 2002; Dall'Olmo et al., 2005;
78 Doxaran et al., 2002; Gitelson et al,. 2008; Morel and Gentili, 2009). These algorithms are generally
79 composed of two key steps. The first step is to develop an index, which could be the reflectance of a
80 single band or the arithmetic combination of reflectance from several bands, by analyzing the IOPs
81 of water constituents. The second step is to empirically establish and calibrate the relationships
82 between the indices obtained from *in situ* reflectance data or satellite data and water constituent
83 concentrations. The relationship could be a linear function (Ammenberg et al., 2002; Gitelson et al.,
84 2008), power function (Kutser et al., 2005), or polynomial function (Dall'Olmo et al., 2003),

depending on the regression analysis and the dynamic ranges in the calibration data used. Since these proposed indices are based on the spectral analysis of IOP for each OAS, they can effectively minimize the effects of the other OASs on the OAS of interest. Therefore, the algorithms based on these indices not only promise improved performance for predicting the water constituent concentration of interest but also are easy to implement using satellite data. However, there still are two major challenges in the application of the semi-analytical algorithms. First, the models for estimation of water constituent concentrations depend greatly on the calibration process; thus, a dataset without a sampling bias is needed to calibrate these models. Second, the proposed indices were developed based on several specific assumptions, some of which may not be universally applicable. For example, an important assumption in the three-band index for estimating chlorophyll *a* concentration is that the absorption and backscattering of suspended solids at the near-infrared band (750-760 nm) can be neglected compared with the absorption of pure water (Gitelson et al., 2008). However, this assumption is not applicable in some highly turbid case II waters, such as those of Lake Taihu and Lake Dianchi in China and Lake Kasumigaura in Japan, and thus resulted in large errors in chlorophyll *a* concentration estimates in these lakes (Le et al., 2009; Yang et al., 2010).

Consequently, the main objective of the present study was to propose a novel method by integrating several semi-analytical algorithms with a look-up-table method to address the two challenges described above. To evaluate the performances of the proposed method, three datasets obtained from bio-optical model simulation, field surveys and Medium Resolution Imaging Spectrometer (MERIS) data were used in this study.

2. Methods

2.1 Bio-optical model

According to Gordon et al. (1975), the remote-sensing reflectance just beneath the water surface can be expressed as:

$$R_{rs}(\lambda,0^{-}) = \frac{f}{Q} \times \frac{b_b(\lambda)}{a(\lambda)+b_b(\lambda)} \quad (1)$$

where $a(\lambda)$ and $b_b(\lambda)$ are the spectral total absorption and backscattering coefficients, respectively, f is the anisotropic factor of the downwelling light field; and Q is the geometrical factor. Austin (1980) proposed the factor of 0.544 for relating radiance just above the surface to radiance just beneath the surface. Thus, remote-sensing reflectance just above the water surface is determined as follows:

$$R_{rs}(\lambda) = 0.544 \times \frac{f}{Q} \times \frac{b_b(\lambda)}{a(\lambda)+b_b(\lambda)} \quad (2)$$

Kirk (1994) found that f is a function of the solar elevation angle that was reasonably well expressed as a linear function of μ_0, the mean cosine of the zenith angle of the refracted photons as follows:

$$f = 0.975 - 0.629\mu_0 . \quad (3)$$

The value of μ_0 depends on the solar elevation and the proportion of direct and diffuse radiations. It is calculated according to the sampling time, locations and solar zenith angle. Q is usually expected to range from 3 to 4 (Morel and Gentili, 1993). Gons (1999) proposed an empirical equation of $Q=2.38/\mu_0$ for turbid inland waters under different solar elevation angles. This equation has been successfully applied for modeling remote-sensing reflectance in an extremely turbid case II water (i.e. Lake Taihu, China; Zhang et al., 2009). Since Lake Dianchi is also a turbid lake, the same equation was used in this study.

127 The spectral total absorption coefficient, $a(\lambda)$, is usually expressed as the sum of the
128 constituents' absorption coefficients, as follows:

129 $$a(\lambda) = a_{\mathrm{w}}(\lambda) + [\mathrm{Chl-a}]a^{*}_{\mathrm{ph}}(\lambda) + [\mathrm{TR}]a^{*}_{\mathrm{tr}}(\lambda) + [\mathrm{CDOM}]a^{*}_{\mathrm{CDOM}}(\lambda), \quad (4)$$

130 where [Chl-a] and [TR] denote concentrations of chlorophyll *a* and tripton, respectively; [CDOM]
131 denotes the absorption of CDOM at 440 nm; $a_{\mathrm{w}}(\lambda)$ is the absorption coefficient of pure water; and
132 $a^{*}_{\mathrm{ph}}(\lambda)$, $a^{*}_{\mathrm{tr}}(\lambda)$ and $a^{*}_{\mathrm{CDOM}}(\lambda)$ are specific absorption coefficients for phytoplankton, tripton and
133 CDOM, respectively. The spectral total backscattering coefficient is expressed as the sum of the
134 backscattering coefficients for each constituent in water except for CDOM, as follows:

135 $$b_{\mathrm{b}}(\lambda) = b_{\mathrm{b,w}}(\lambda) + [\mathrm{Chl-a}]b^{*}_{\mathrm{b,ph}}(\lambda) + [\mathrm{TR}]b^{*}_{\mathrm{b,tr}}(\lambda), \quad (5)$$

136 where $b_{\mathrm{b,w}}(\lambda)$ is the backscattering coefficient of pure water, and $b^{*}_{\mathrm{b,ph}}(\lambda)$ and $b^{*}_{\mathrm{b,tr}}(\lambda)$ are the
137 backscattering coefficients for phytoplankton and tripton, respectively.

138 ***2.2*** **Study areas and *In situ* data**

139 Field investigations were carried out in Lake Dianchi (24°50′N; 102°41′E) and Lake
140 Kasumigaura (36°00′N; 140°25′E). Lake Dianchi is located in a plateau area of the southwestern
141 part of China (Fig.1A). It has a surface area of 300 km^2 and is the largest lake in Yunnan Province
142 and the sixth largest lake in China. The mean depth of the lake is 4.3 m and the maximum depth is
143 11.3 m. Eutrophication has become more and more serious in the lake in the recent 20 years due to
144 the large quantities of industrial wastewater and municipal sewage discharged into the lake; algal
145 blooms occur frequently from April to November each year (Gao et al., 2005). Lake Kasumigaura is
146 located in the eastern part of Japan's Kanto Plain (Fig.1B). It is the second largest lake of Japan, with
147 a surface area of 171 km^2 and an average depth of 4 m (maximum depth of 7.3 m). The lake is

148 considered eutrophic, because is has a high load of nutrients, and because of its shallow depth
149 (Fukushima et al., 1996).
150
151 ---------- Please insert Fig. 1 here ----------
152
153 Three data collection campaigns were undertaken in 2007 (Oct. 23) and 2009 (Mar. 12 and Jul.
154 24-31) in Lake Dianchi; and other two campaigns were undertaken in 2006 (Feb. 18) and 2008 (Aug.
155 07) in Lake Kasumigaura. The spatial distribution of sampling sites is shown in Fig. 1. Sample
156 collections and reflectance measurements were performed between 10:00 and 14:00 h local time.
157 Water samples were kept in ice boxes and taken to the laboratory within approximately 0.5 hours
158 after whole data collections. Chlorophyll *a* was extracted using methanol (100%) at 4^{o}C under dark
159 conditions for 24 hours. The optical density of the extracted chlorophyll *a* was measured at four
160 wavelengths (750, 663, 645 and 630 nm) and the concentration was calculated according to
161 SCOR-UNESCO equations (SCOR-UNESCO, 1966). To obtain the concentration of tripton, the
162 total suspended solids (TSS) were divided into tripton and phytoplanktonic suspended solids (PSS).
163 Based on the method of Gons et al. (1992) and organic suspended solids (OSS) data collected from
164 two lakes, it can be assumed that 1 mg m^{-3} chlorophyll *a* concentration is approximately equal to
165 0.148 g m^{-3} TSS in Lake Dianchi and 0.12 g m^{-3} TSS in Lake Kasumigaura. Tripton concentrations
166 were then derived by subtracting PSS from TSS. The absorption of CDOM was measured using a
167 Shimadzu UV-1700 spectrophotometer with filtered water. *In situ* reflectance spectra were collected
168 according to Method 1 of Mueller et al. (2000).

2.3 Estimation of SIOPs

Four water samples collected from Lake Dianchi under a very clear sky and low wind speed in Jul. 2009 were used to measure/estimate the absorption and backscattering spectra for CDOM, phytoplankton and tripton. The corresponding remote-sensing reflectance spectra were also collected at these four sites to estimate the backscattering spectra for phytoplankton and tripton by the method that will be described below. The absorption coefficients of tripton ($a_{tr}(\lambda)$), CDOM ($a_{CDOM}(\lambda)$) and phytoplankton ($a_{ph}(\lambda)$) were determined according to the quantitative filter technique (QFT) (Mitchell, 1990).

As demonstrated in Giardino et al. (2007), the specific absorption of tripton, $a^*_{tr}(\lambda)$, could be fitted with an exponential wavelength function as follows:

$$a^*_{tr}(\lambda) = a^*_{tr}(440)\exp[-S_{tr}(\lambda - 440)] \quad (6)$$

where $a^*_{tr}(440)$ is the specific absorption of tripton at 440 nm and S_{tr} is the shape factor of the absorption of tripton. Here, $a^*_{tr}(440)$ and S_{tr} equal 0.0683 and 0.0115, respectively. The specific absorption of CDOM, $a^*_{CDOM}(\lambda)$, can also be described as an exponential function as follows:

$$a^*_{CDOM}(\lambda) = a^*_{CDOM}(440)\exp[-S_{CDOM}(\lambda - 440)], \quad (7)$$

where S_{CDOM} is the shape factor of the absorption spectra of CDOM. The value of $a^*_{CDOM}(440)$ equals 1 since the absorption spectra of CDOM is normalized by the absorption coefficient at 440 nm; S_{CDOM} equals 0.0157 according to the best-fit results for the *in situ* collected data of this study. The absorption coefficient of pure water, $a_w(\lambda)$, was taken from Hale and Querry (1973) and Pope and Fry (1997).

The backscattering coefficients were obtained based on an inversion of the bio-optical model

used in this study. According to equations 2 and 5, the backscattering coefficient of particles (including phytoplankton and tripton), $b_{b,p}(\lambda)$, can be obtained as follows:

$$b_{b,p}(\lambda) = \frac{a(\lambda)R_{rs}(\lambda)}{0.544(f/Q) - R_{rs}(\lambda)} - b_{b,w}(\lambda), \quad (8)$$

where $b_{b,w}(\lambda)$ is the backscattering coefficient of pure water cited from Morel (1974).

The separation of phytoplankton and tripton backscattering is based on the assumption that contributions of backscattering due to phytoplankton cells and tripton are proportional to the ratios of their masses (Brando and Dekker, 2003). As the total backscattering of particles can be derived from Eq. 8, specific backscattering coefficients for these two components can be retrieved. According to Giardino et al. (2007), the specific backscattering coefficient of tripton, $b^*_{b,tr}(\lambda)$, can also be found from following equation:

$$b^*_{b,tr}(\lambda) = b^*_{b,tr}(550)\left(\frac{\lambda}{550}\right)^{-n}, \quad (9)$$

where $b^*_{b,tr}(550)$ is the specific backscattering coefficient of tripton at 550 nm, and n is an exponent describing the spectral dependency of tripton backscattering (Giardino et al., 2007). Here, $b^*_{b,tr}(550)$ and n equals 0.0116 and 0.7744, respectively. Fig. 2 shows the specific inherent optical properties (SIOPs) for each component collected in Lake Dianchi.

---------- Please insert Fig. 2 here ----------

The measured and modeled $R_{rs}(\lambda)$ at two additional sites were compared to validate the estimated SIOPs of Lake Dianchi (Fig. 3). The two sites had moderate (59.29 mg m^{-3}) and high

(131.79 mg m^{-3}) concentrations of chlorophyll *a*. The results show strong agreement between the measured and modeled $R_{rs}(\lambda)$, suggesting that the measured specific absorption coefficients and retrieved specific backscattering coefficients are determined reasonably well.

---------- Please insert Fig. 3 here ----------

2.4 MERIS data collection

Two full-resolution MERIS images (level-1b) covering Lake Dianchi were acquired on Oct. 24, 2007 (orbit 29531, starting time 03:32:09 UTC) and Mar. 13, 2009 (orbit 36774, starting time 03:29:13 UTC), which were each one day after the date of the corresponding field survey (Fig. 1A). Other two full-resolution MERIS images covering Lake Kasumigaura were acquired on Feb. 18, 2006 (orbit 20775, starting time 01:15:29 UTC) and Aug. 7, 2008 (orbit 33652, starting time 00:56:50 UTC), on which the two field campaigns were carried out (Fig. 1B). Images were analyzed using BEAM 4.0 software (Brockmann Consult, Geesthacht, Germany). The images were geo-located and masked for land, clouds and invalid reflectance. Atmospheric correction was performed using the SCAPE-M (Self-Contained Atmospheric Parameters Estimation for MERIS data) atmospheric processor, which outperformed other previous atmospheric correction algorithms for turbid inland lakes (Guanter et al., 2010).

3. Development of a novel method for retrieving water constituent concentrations

3.1 Performances of the original semi-analytical algorithms

Among a number of semi-analytical indices proposed for case II waters, three indices were selected for further investigation based on their reasonableness and performance as reported in previous studies (Ammenberg et al., 2002; Gitelson et al., 2008).

A three-band index proposed by Gitelson et al. (2008) was first selected to estimate chlorophyll *a* concentration in case II waters. This index requires the reflectance at three bands as input, i.e., λ_1=660-670 nm, λ_2=700-730 nm, λ_3=740-760 nm. The selection of these bands is based on three assumptions: (1) the chlorophyll *a* absorption in the first band, λ_1, should be much larger than that in the second band, λ_2; that is, $a_{Chla}(\lambda_1) >> a_{Chla}(\lambda_2)$; (2) the tripton and CDOM absorption in the first band, λ_1, should be similar to that in the second band, λ_2; that is, $a_{tr}(\lambda_1) \approx a_{tr}(\lambda_2)$, $a_{CDOM}(\lambda_1) \approx a_{CDOM}(\lambda_2)$; (3) the third band, λ_3, should be minimally affected by the total backscattering and the absorption of phytoplankton, tripton and CDOM, but should have similar backscattering to those of the first and second bands; that is, $a_w(\lambda_3) >> a_{ph}(\lambda_3) + a_{tr}(\lambda_3) + a_{CDOM}(\lambda_3) + b_b(\lambda_3)$, $b_b(\lambda_3) \approx b_b(\lambda_2) \approx b_b(\lambda_1)$. Thus, the three-band index relating [Chl-a] can be expressed as follows:

$$\begin{aligned} & [R_{rs}^{-1}(\lambda_1) - R_{rs}^{-1}(\lambda_2)] \times R_{rs}(\lambda_3) \\ & \propto [a_{Chla}(\lambda_1) + a_w(\lambda_1) - a_w(\lambda_2)] / a_w(\lambda_3) \\ & \propto [\text{Chl} - \text{a}] \end{aligned} \quad (10)$$

The remote-sensing reflectance in the near-infrared (NIR) band was selected to estimate the concentration of tripton (Ammenberg et al., 2002). Generally, backscattering of tripton is noticeably larger than that of phytoplankton; that is, $b_{b,tr}(\lambda_{NIR}) >> b_{b,ph}(\lambda_{NIR})$. In the NIR region (700-800 nm), the total absorption was approximately equal to the absorption by pure water; that is, $a_{total}(\lambda_{NIR}) \approx a_w(\lambda_{NIR})$. The absorption of pure water is also much larger than the backscattering of particles

($a_w(\lambda_{NIR}) >> b_{b,p}(\lambda_{NIR})$) (e.g., Babin and Stramski, 2002; Gitelson et al,. 2008; Gons, 1999). Thus, the remote-sensing reflectance in the NIR band relating [TR] can be expressed as follows:

$$\begin{aligned} R_{rs}(\lambda_{NIR}) &= \frac{f}{Q} \times \frac{b_{b,w}(\lambda_{NIR}) + b_{b,tr}(\lambda_{NIR}) + b_{b,ph}(\lambda_{NIR})}{a_{total}(\lambda_{NIR}) + b_{b,tr}(\lambda_{NIR}) + b_{b,ph}(\lambda_{NIR}) + b_{b,w}(\lambda_{NIR})} \\ &\approx \frac{f}{Q} \times \frac{b_{b,w}(\lambda_{NIR}) + b_{b,tr}(\lambda_{NIR})}{a_w(\lambda_{NIR})} \\ &\propto [TR] \end{aligned} \quad (11)$$

A band-ratio index proposed by Ammenberg et al. (2002) was selected to estimate the absorption of CDOM at 440 nm. The relationship between the index and [CDOM] is expressed as follows:

$$R_{rs}(664) / R_{rs}(550) \quad \propto \quad [CDOM] \quad (12)$$

$R_{rs}(550)$ is influenced by the absorption of CDOM, as well as scattering by all aprticular matters, but it is not strongly influenced by the absorption of chlorophyll, while $R_{rs}(664)$ is affected by both the absorption of chlorophyll and the backscattering by phytoplankton and tripton. Using $R_{rs}(664)$ in the numerator of the band ratio therefore normalizes for variations in both phytoplankton absorption and for the effects of variations in backscattering (Ammenberg et al., 2002).

To thoroughly investigate the performances of these semi-analytical algorithms, a reflectance spectra dataset was generated using the SIOPs and the bio-optical model described above. The average value of f/Q (0.156) obtained from the *in situ* data in Lake Dianchi was used in the spectra generation. The concentrations of chlorophyll *a* ([Chl-a]) and tripton ([TR]), as well as the absorption of CDOM at 440 nm ([CDOM]) were varied in the ranges of 1-300 (mg m^{-3}), 1-250 (g m^{-3}) and 0.1-10 (m^{-1}), respectively. Similar with increments used in Kutser et al. (2006), the increment of constituent concentrations varied for different ranges. For [Chl-a], an increment of 1 mg m^{-3} was used in the range of 1-10 mg m^{-3}, an increment of 2 mg m^{-3} was used in the range of

269 10-20 mg m^{-3}, an increment of 10 mg m^{-3} was used in the range of 20-60 mg m^{-3} and an increment of
270 20 mg m^{-3} was used in the range of 60-300 mg m^{-3}. For [TR], the increments of 1 g m^{-3}, 5 g m^{-3} and
271 20 g m^{-3} were used in the ranges of 1-10 g m^{-3}, 10-50 g m^{-3} and 50-250 g m^{-3}, respectively. For
272 [CDOM], the increments of 0.1 m^{-1}, 0.5 m^{-1} and 1 m^{-1} were used in the ranges of 0.1-1.0 m^{-1}, 1.0-5.0
273 m^{-1} and 5.0-10.0 m^{-1}, respectively. Thus, 19,964 (i.e., 31×28×23) sample spectra in total were
274 generated to establish the relationships between the indices and water constituent concentrations.
275 Since the MERIS sensor has great potential in the remote sensing of case II waters, the generated
276 spectra were resampled to MERIS bandwidths (shown in Table 1) through corresponding spectral
277 response functions to calculate the semi-analytical indices.
278
279 ---------- Please insert Table 1 here ----------
280
281 Through regression analysis between the indices and constituent concentrations, the initial
282 estimation models for [Chl-a], [TR] and [CDOM] could be obtained (Fig. 4):

283 $$[\text{Chl}-\text{a}] = 223.86\left[R_{\text{rs}}(\text{b}_{10})/R_{\text{rs}}(\text{b}_7) - R_{\text{rs}}(\text{b}_{10})/R_{\text{rs}}(\text{b}_9)\right] + 23.95 \quad (13)$$

284 $$[\text{TR}] = 49909R_{\text{rs}}^2(\text{b}_{10}) - 61.38R_{\text{rs}}(\text{b}_{10}) + 4.74 \quad (14)$$

285 $$[\text{CDOM}] = 3.03\left[R_{\text{rs}}(\text{b}_7)/R_{\text{rs}}(\text{b}_5)\right] + 0.35, \quad (15)$$

286 where b_5, b_7, b_9 and b_{10} denote the bandwidths of MERIS bands 5 (555-565 nm), 7 (660-670 nm), 9
287 (703.75-713.75 nm) and 10 (750-757.5 nm), respectively. It is clearly seen that the assumptions in
288 the indices development process resulted in larger errors in the estimations of the water constituent
289 concentrations, even though noise-free simulation data was used. Especially for [CDOM] estimation,

290 a poor R^2 was given (Fig. 4C). This is because the $R_{rs}(550)$ will be influenced by chlorophyll
291 absorption for samples with high [Chl-a].
292
293 ---------- Please insert Fig.4 here ----------
294
295 To improve the performances of the semi-analytical algorithms, the bio-optical model was
296 theoretically reanalyzed. From equations (1), (4) and (5), it can be seen that the remote-sensing
297 reflectance in case II waters depends on concentrations of three constituents: phytoplankton, tripton
298 and CDOM (absorption and backscattering coefficients of pure water are usually treated as
299 constants). As in a microcosm experiment (i.e., making an artificial ecosystem in which some
300 conditions are controlled to simulate behaviors of a simplified natural ecosystem; e.g., Hunter et al.,
301 2008), we can consider an imaginary case II water, in which only one constituent changes while the
302 other two constituents are controlled as constants. For example, the imaginary case II water has
303 variable concentrations of chlorophyll *a* but constant concentrations of tripton and CDOM. The
304 changes of remote-sensing reflectance in this imaginary case II water should only depend on the
305 changes of the chlorophyll *a* concentration. In this case, the chlorophyll *a* concentration should also
306 be accurately predicted by a semi-analytical index calculated from the remote-sensing reflectance.
307 Fig. 5A shows the relationships between chlorophyll *a* concentration and the three-band index, with
308 a constant tripton concentration and CDOM absorption of low, moderate and high values,
309 respectively. As the figure shows, by using quadratic functions, accurate estimation models of
310 [Chl-a] can be constructed by regression analysis (correlation coefficients equal to 1 and root mean

311 square error (RMSE) around 0). For other combinations of [TR] and [CDOM] not shown in Fig.5A,
312 the regressions were all statistically significant with R^2 > 0.99 and *P*-value << 0.0001. This
313 phenomenon provides a good opportunity to avoid the estimation errors of chlorophyll *a*
314 concentration due to the assumptions in the index development process. Similar results for the
315 estimation of tripton concentration and CDOM absorption coefficient can also be obtained, as shown
316 in Fig. 5B and 5C, respectively.

317 It is noted that the index of $R_{rs}(b_7)/R_{rs}(b_5)$ is not sensitive to variation of [CDOM] when [Chl-a]
318 and [TR] are relatively high (e.g., cases II and III in Fig. 5C with [Chl-a] = 100 mg m^{-3} , [TR] = 90 g
319 m^{-3} and [Chl-a] = 300 mg m^{-3}, [TR] = 250 g m^{-3}, respectively). In these cases, the optical properties
320 of the water are dominated by particles (i.e. tripton and phytoplankton). Therefore, variation of
321 [CDOM] will not largely change the reflectance and thus is not sensitive to the semi-analytical
322 index.

323

324 ---------- Please insert Fig.5 here ----------

325

326 ***3.2 Semi-analytical model optimizing and look-up tables***

327 As shown in Fig. 5, unlike the case using the original semi-analytical algorithms, polynomial
328 functions are needed to represent the relationships between semi-analytical indices and water
329 constituent concentrations. These relationships can be expressed as follows:

330 $$[\text{Chl}-\text{a}] = pX_{\text{ph}}^{\ 2} + qX_{\text{ph}} + r \quad (16)$$

331 $$[\text{TR}] = aX_{\text{tr}}^{\ 3} + bX_{\text{tr}}^{\ 2} + cX_{\text{tr}} + d \quad (17)$$

$$[\mathrm{CDOM}] = mX_{\mathrm{CDOM}}^{2} + nX_{\mathrm{CDOM}} + h \quad (18)$$

where X_{ph}, X_{tr} and X_{CDOM} denote the indices $R_{\mathrm{rs}}(\mathrm{b}_{10})/R_{\mathrm{rs}}(\mathrm{b}_{7}) - R_{\mathrm{rs}}(\mathrm{b}_{10})/R_{\mathrm{rs}}(\mathrm{b}_{9})$, $R_{\mathrm{rs}}(\mathrm{b}_{10})$ and $R_{\mathrm{rs}}(\mathrm{b}_{7})/R_{\mathrm{rs}}(\mathrm{b}_{5})$ for chlorophyll *a*, tripton and CDOM, respectively. The regression coefficients *p*, *q* and *r* are determined according to [TR] and [CDOM]; *a*, *b*, *c* and *d* are determined according to [Chl-a] and [CDOM]; and *m*, *n* and *h* are determined according to [Chl-a] and [TR], respectively. These regression coefficients can be determined for different concentration combinations of any two constituents with fine concentration intervals to represent any case of waters, through simulated reflectance spectra based on the bio-optical model. For example, in the case of estimating [Chl-a], increments of 1 g m^{-3} and 0.1 m^{-1} were used in the ranges of 1-250 g m^{-3} and 0.1-10 m^{-1} for [TR] and [CDOM], respectively; while increments for [Chl-a] were the same as those shown in Fig. 5A. Thus, 250×100×31 sample spectra in total were generated to establish the relationships between the three-band index and [Chl-a]. Correspondingly, increments of 1 mg m^{-3} and 0.1 m^{-1} for [Chl-a] and [CDOM] were used for the estimation models of [TR]; increments of 1 mg m^{-3} and 1 g m^{-3} for [Chl-a] and [TR] were used for the estimation models of [CDOM]. In the end, three 2-dimensional look-up tables (LUTs) were constructed, containing the coefficients of the estimation model for one constituent of interest determined by the concentrations of other two constituents. Table 2 shows an example of the LUT for estimation models of chlorophyll *a* concentration.

---------- Please insert Table 2 here ----------

A practical problem is that any information on water constituent concentrations is unknown for

353 a given pixel of satellite data, except for the remote-sensing reflectance. Thus, it is impossible to
354 determine which estimation model is the most appropriate for an index calculated for this pixel. To
355 solve this problem, a method based on semi-analytical model optimizing and look-up tables
356 (SAMO-LUT) is proposed. Fig. 6 shows the major steps of the SAMO-LUT method as follows:

357 Step 1 is to calculate the selected semi-analytical indices for the corresponding concentrations
358 of chlorophyll *a*, tripton and CDOM.

359 Step 2 is to obtain initial estimations of chlorophyll *a* concentration ($[\text{Chl-a}]_0$ in Fig. 6), tripton
360 concentration ($[\text{TR}]_0$ in Fig. 6) and the CDOM absorption coefficient at 440 nm ($[\text{CDOM}]_0$ in Fig. 6)
361 using equations 13-15.

362 Step 3 is to find an estimation model (i.e., regression coefficients of Equations 16-18 saved in
363 the LUT) from the LUTs for each water constituent using the known initial values of $[\text{Chl-a}]_0$ and
364 $[\text{TR}]_0$ obtained in step 2, then use the chosen estimation models to replace the previous ones
365 (Equations 13-15). The new concentrations of chlorophyll *a* and tripton ($[\text{Chl-a}]_1$ and $[\text{TR}]_1$ in Fig.
366 6) and the CDOM absorption coefficient at 440 nm ($[\text{CDOM}]_1$ in Fig. 6) are then recalculated,
367 respectively.

368 Step 4 is to find a more appropriate estimation model from the LUTs for each water constituent
369 through the iterative use of the newly obtained concentrations of chlorophyll *a* and tripton and the
370 CDOM absorption coefficient at 440 nm instead of the previous values. For example, $[\text{Chl-a}]_1$, $[\text{TR}]_1$
371 and $[\text{CDOM}]_1$ were used instead of $[\text{Chl-a}]_0$, $[\text{TR}]_0$ and $[\text{CDOM}]_0$ in the second iteration,
372 respectively (Fig. 6). The new concentrations of chlorophyll *a* and tripton ($[\text{Chl-a}]_2$ and $[\text{TR}]_2$ in Fig.
373 6) and the CDOM absorption coefficient at 440 nm ($[\text{CDOM}]_2$ in Fig. 6) were then calculated again.

374

375 ---------- Please insert Fig.6 here ----------

376

377 The iteration will be ended when the difference between the current and last outputs is
378 adequately small. In this study, the RMSE of the estimated water constituent concentrations in the
379 *n*-th and (*n*-1)-th iteration was used as the criterion to determine the appropriate number of iterations.
380 The RMSEs become stable after the 10th iteration. Therefore, the estimated water constituent
381 concentrations with 10 iterations were used as the final results in the validation process.

382

383 ## 4. Validation results and discussion

384 ### *4.1 Validation with simulation data*

385 A validation dataset was generated separately from the dataset used for the calibrations of the
386 estimation models using a different sampling strategy. The concentrations of chlorophyll *a* and
387 tripton as well as the absorption coefficient of CDOM at 440 nm were varied with a random
388 distribution in the ranges of 0-300 (mg m^{-3}), 0-250 (g m^{-3}) and 0-10 (m^{-1}), respectively. The 1000
389 simulated reflectance spectra were resampled to the bandwidths of MERIS channels.

390 Three indices, namely the root mean square error (RMSE), mean normalized bias (MNB) and
391 normalized root mean square error (NRMS), were used in accuracy assessment, as suggested by
392 Gitelson et al. (2008). These indices are defined as follows:

393 $$\mathrm{RMSE} = \sqrt{\frac{\sum_{i=1}^{N}(X_{\mathrm{esti,i}} - X_{\mathrm{meas,i}})^2}{N}} \quad (19)$$

$$\mathrm{MNB} = mean(\varepsilon_i)\% \quad \text{and} \tag{20}$$

$$\mathrm{NRMS} = stdev(\varepsilon_i)\%, \tag{21}$$

where $X_{esti,i}$ and $X_{meas,i}$ are the estimated and measured values, respectively; N is the number of samples; $\varepsilon_i=100\times(X_{esti,i}-X_{meas,i})/X_{meas,i}$ is the percent difference between the estimated and measured values. The MNB denotes the average bias in the estimation, while the NRMS denotes the relative random uncertainty of the results. The coefficient of determination (R^2) between $X_{esti,i}$ and $X_{meas,i}$ is also calculated.

Scatter plots of estimated and true water constituent concentrations are shown in Fig. 7, and the assessment results are summarized in Table 3. The results show that the SAMO-LUT method works very well for the simulated spectra with MNB < 1.74%, NRMS < 8.12% and small RMSE values close to 0 mg m^{-3} (or g m^{-3} or m^{-1}). In addition, the coefficients of determination (R^2) and slopes and intercepts of the regression analysis between the true and estimated values were around 1.0, 1.0 and 0, respectively (Fig. 7). These results indicate that the SAMO-LUT method is a reasonable approach.

---------- Please insert Fig. 7 here ----------

To further demonstrate the performance of the proposed method, the three previously presented semi-analytical algorithms for estimating [Chl-a], [TR] and [CDOM] (Eqs. 13-15) were also assessed using the same validation dataset. The results are summarized in Table 3. Estimation results show noticeable errors for these methods with average bias (MNB) and relative random uncertainty (NRMS) in the range of 15.26%–139.62% and 328.84%–1160.92%, respectively.

415

416 ---------- Please insert Table 3 here ----------

417

418 These results indicate that: (1) the estimation error due to the assumptions in the development
419 process of a semi-analytical index cannot be ignored in many case II waters; and (2) the calibration
420 process strongly depends on the dataset used. For example, if several randomly generated datasets
421 were used to calibrate models for [Chl-a] estimation, different [Chl-a] estimation models will usually
422 be obtained. This is because the assumptions will introduce different effects for different water
423 samples, then resulting in different indices values even for some water samples with the same
424 [Chl-a] values. This is also why some semi-analytical algorithms were site-specific ones.

425 In contrast, the results obtained from the SAMO-LUT method indicate that the above problems
426 can be solved by using the semi-analytical indices for each special case (i.e., a set of samples with
427 only one water constituent concentration changed; see Fig. 5) and iteratively searching the most
428 appropriate estimation model (optimization) from a prepared LUT for a given case. Since the effects
429 caused by the assumptions in a semi-analytical index are constants for each special case, the
430 estimation model for each special case can be accurately calibrated. These estimation models can be
431 easily constructed using the simulation data rather than using the data collected from the field
432 investigations, because it is difficult or impossible to collect enough data from actual waters to cover
433 all special cases, whereas the simulation data can be generated under any desired environmental
434 conditions. The optimization process allows us to gradually refine the estimation model for each
435 water constituent concentration and finally to obtain the most accurate results.

4.2 Validation with in situ *data*

In situ data collected from Lake Dianchi in Jul., 2009 (19 samples) was also used to validate the SAMO-LUT method. The results are shown in Fig. 8 and Table 3. It can be seen that the SAMO-LUT method performed well even for these *in situ* collected data. The RMSE, MNB and NRMS were 3.37 mg m^{-3}, -1.58% and 3.65% for the [Chl-a] estimation; 1.81 g m^{-3}, 3.83% and 6.73% for the [TR] estimation, and 0.21 m^{-1}, -7.07% and 31.19% for the [CDOM] estimation, respectively. The determination coefficients were 0.98 for the [Chl-a] estimation, 0.89 for the [TR] estimation and 0.78 for the [CDOM] estimation.

---------- Please insert Fig. 8 here ----------

The results obtained from the *in situ* data showed less accuracy for each water constituent concentration compared with those obtained from the simulation data. This is probably because of biases in the optical closure processes. Optical closure refers to the testing of the theoretical interrelationship between measured inherent optical properties (IOPs) and apparent optical properties (AOPs) of a water body (Gallegos et al., 2008). Since calibration of the semi-analytical models is based on simulation data, optical closure plays a crucial role in the successful application of the SAMO-LUT method. In this study, SIOPs were measured or estimated from four sampling sites in Lake Dianchi and then were assumed as constants for the whole lake. Results shown in Figs. 3 and 8 indicate this assumption is reasonable in the study areas. In addition, compared with the simulation data, measurement errors included in the *in situ* data can also result in relatively larger estimation

457 errors.

458 The semi-analytical algorithms were also applied to the *in situ* data. Since the relationships
459 between semi-analytical indices and water constituent concentrations in the semi-analytical
460 algorithms strongly depend on the calibration dataset used (e.g., dynamic range and number of data),
461 the semi-analytical algorithms established from the simulation dataset (i.e. Eqs. 13-15) were applied
462 to the *in situ* data for fair comparisons rather than using the *in situ* data for model calibration. The
463 results show that the estimation accuracy for [Chl-a] was slightly decreased (the RMSE, MNB and
464 NRMS were 3.60 mg m^{-3}, -1.77% and 4.06%, respectively). However, the estimation accuracies for
465 [TR] and [CDOM] were dramatically reduced compared with those of the SAMO-LUT (Table 3, the
466 RMSE, MNB and NRMS were 8.50 mg m^{-3}, -4.49% and 35.87% for [TR] and 1.42 m^{-1}, 388.64%
467 and 375.26% for [CDOM], respectively). The poor performances of the semi-analytical algorithms
468 were mainly caused by the invalid assumptions in the semi-analytical indices.

469

470 ***4.3 Validation with MERIS data***

471 Two MERIS images for Lake Dianchi and other two MERIS images for Lake Kasumigaura (as
472 shown in Fig.1) were used to further validate the SAMO-LUT method. Pixels contaminated by
473 clouds were excluded; and only sampling sites located more than one pixel away from the bank were
474 remained. Accordingly, there are 21 and 18 sites remained for Lake Kasumigaura in Feb. 2006 and
475 Aug. 2008, respectively (25 sampling sites in total for both field works). For Lake Dianchi, there are
476 3 and 5 sites available in Oct. 2007 and Mar. 2009, respectively. To enable comparison with *in situ*
477 reflectance, the average reflectance of the pixel nearest to the sampling location along with the 8

surrounding pixels was computed. These 9 pixels represent a surface area of approximately 0.8 km^2. A comparison of *in situ* and atmospherically corrected satellite reflectance for Lake Dianchi is shown in Fig. 9. The results of atmospheric correction are acceptable with high agreement between the *in situ* and MERIS-derived remote-sensing reflectance spectra. For Lake Kashumigaura, similar results were obtained (data not shown).

---------- Please insert Fig. 9 here ----------

Fig. 10 and Table 3 show the performance of the SAMO-LUT method for the MERIS data. It should be noted that the CDOM measurements were unavailable for Lake Kasumigaura on Feb. 18, 2006. The MERIS-derived constituent concentrations were in good agreement with *in situ* measured values with all the points close to the 1:1 line (Fig. 10). The RMSE, MNB and NRMS were 12.64 mg m^{-3}, 7.58% and 16.81% for the [Chl-a] estimation, 4.44 g m^{-3}, -2.85% and 23.32% for the [TR] estimation, and 0.32 m^{-1}, 8.74% and 33.62% for the [CDOM] estimation, respectively (Table 3). The determination coefficients were 0.76 for the [Chl-a] estimation, 0.89 for the [TR] estimation and 0.26 for the [CDOM] estimation. The low determination coefficient for the [CDOM] estimation is probably due to errors in the atmospheric corrections for MERIS bands 5 and 7 and its relatively narrow distribution range (0.2-1.5 m^{-1}). The semi-analytical algorithms (Eqs. 13-15) were also used for estimating water constituent concentrations from MERIS data. The SAMO-LUT method noticeably outperformed these algorithms (Table 3). The [CDOM] showed the lowest accuracy with MNB and NRMS larger than 110%. The estimations of [TR] and

[Chl-a] from semi-analytical algorithms yielded noticeably larger RMSE, MNB and NRMS values than those from the SAMO-LUT method.

---------- Please insert Fig. 10 here ----------

It is noted that the estimation accuracy yielded by the SAMO-LUT method for satellite data is lower than those for both the *in situ* and simulated datasets. The largest error source in the application of satellite image is the atmospheric correction procedure. Although the results shown in Fig. 9 suggest that SCAPE-M is a feasible atmospheric correction algorithm, improving the atmospheric corrections for case II waters is still a challenge due to the complex aerosol composition, sun glint, adjacency effect and others. Therefore, the three indices used in the SAMO-LUT (Eqs. 10-12) were still contaminated by atmosphere due to the imperfect atmospheric corrections, and then limited estimation accuracy of the SAMO-LUT. If the atmospheric factor could be more effectively accounted for, more accurate and reliable monitoring of water quality could be derived from satellite images.

The presented results indicate that the same LUT can be used to estimate water constituent concentrations in two different lakes and periods. This is probably because the SIOPs were similar in the two lakes during the study periods. The SAMO-LUT has the potential to be implemented in other applications, such as case II waters with different SIOPs or use of different satellite sensors. In this case, the look-up tables need to be reconstructed accordingly. This process will be investigated in a future work.

5. Conclusions

In this study, a semi-analytical model optimizing and look-up table (SAMO-LUT) method was proposed to retrieve water constituent concentrations in case II waters. The SAMO-LUT method is based on three previous semi-analytical indices for estimating chlorophyll *a*, tripton and CDOM. The semi-analytical algorithms were optimized based on the fact that estimation of one constituent of interest can be highly improved when the other two constituents' concentrations are known in advance. Look-up tables and an iterative searching strategy were applied to obtain the most appropriate parameters in the estimation models. Three datasets (i.e., noise-free simulation data, *in situ* collected data and MERIS data) were used to validate the performance of the proposed method. The results show that the SAMO-LUT method yields error-free results for the ideal simulation dataset and can also estimate the water constituent concentrations with an average bias (MNB) lower than 9% and a relative random uncertainty (NRMS) lower than 34% even for *in situ* and MERIS data. In the application of satellite data, the performance of the SAMO-LUT still depends on the accuracy of atmospheric correction.

Acknowledgement: This research was supported in part by National Natural Science Foundation of China (Grant No. 40871162), by the Grants-in-Aid for Scientific Research of MEXT from Japan (No. 20510003, No. 19404012) and also by the Global Environment Research Fund (M-10) of the Ministry of the Environment, Japan. The authors would like to acknowledge Dr. L. Guanter, who

developed the SCAPE-M processor and performed atmospheric correction on the MEIRS images used in this study. The authors would like to thank the two anonymous reviewers for the useful comments on the manuscript.

References:

Ammenberg, P., Flink, P., Lindell, T., Pierson, D., & Strombeck, N. (2002). Bio-optical modelling combined with remote sensing to assess water quality. *International Journal of Remote Sensing, 23*, 1621-1638

Austin, R.W. (1980). Gulf of Mexico, ocean-colour surface-truth measurements. *Bound.-Layer Meteorol., 18*, 269-285

Ayres, W., Busia, A., Dinar, A., Hirji, R., Lintner, S., McCalla, A., & Robelus, R. (1996). *Integrated lake and reservoir management: World band approach and experience*. Washington, DC.: World Bank

Babin, M., & Stramski, D. (2002). Light absorption by aquatic particles in the near-infrared spectral region. *Limnology and Oceanography, 47*, 911-915

Brando, V.E., & Dekker, A.G. (2003). Satellite hyperspectral remote sensing for estimating estuarine and coastal water quality. *IEEE Transactions on Geoscience and Remote Sensing, 41*, 1378-1387

Dall'Olmo, G., & Gitelson, A.A. (2005). Effect of bio-optical parameter variability on the remote estimation of chlorophyll-a concentration in turbid productive waters: experimental results. *Applied Optics, 44*, 412-422

Dall'Olmo, G., Gitelson, A.A., & Rundquist, D.C. (2003). Towards a unified approach for remote estimation of chlrophyll-a in both terrstrial vegetatioin and turbid productive waters. *Geophysical Reseach Letters, 30*, doi:10.1029/2003GL018065

Doxaran, D., Froidefond, J.M., & Castaing, P. (2002). A reflectance band ratio used to estimate suspended matter concentrations in sediment-dominant coastal waters. *International Journal of Remote Sensing, 23*, 5079–5085

Fukushima, T., Park, J., Imai, A., Matsushige, K. (1996). Dissolved organic carbon in a eutrophic lakes; dynamics, biodegradability and origin. *Aquatic Sciences, 58*, 139-157.

Gallegos, C.L., Davies-Colley, R.J., & Gall, M. (2008). Optical closure in lakes with contrasting extremes of reflectance. *Limnology and Oceanography, 53*, 2021-2034

Gao, L., Zhou, J.M., Yang, H., & Chen, J. (2005). Phosphorus fractions in sediment profiles and their potential contributions to eutrophication in Dianchi Lake. *Environmental Geology, 48*, 835-844

Garver, S., & Siegel, D. (1997). Inherent optical property inversion of ocean color spectra and its biogeochemical interpretation 1. Time series from the Sargasso Sea. *Journal of Geophysical Research-Oceans, 102*, 18607-18625

Giardino, C., Brando, V.E., Dekker, A.G., Strömbeck, N., & Candiani, G. (2007). Assessment of water quality in Lake Garda (Italy) using Hyperion. *Remote Sensing of Environment, 109*, 183-195

579 Gin, K.Y.H., Koh, S.T., & Lin, I.I. (2002). Study of the effect of suspended marine clay on the reflectance
580 spectra of phytoplankton. *International Journal of Remote Sensing, 23,* 2163–2178
581 Gin, K.Y.H., Koh, S.T., & Lin, I.I. (2003). Spectral irradiance profile of suspended marine clay for the
582 estimation of suspended sediment concentration in tropical waters. *International Journal of Remote*
583 *Sensing, 24*, 3235–3245
584 Gitelson, A.A., Dall'Olmo, G., Moses, W., Rundquist, D.C., Barrow, T., Fisher, T.R., Gurlin, D., & Holz, J.
585 (2008). A simple semi-analytical model for remote estimation of chlorophyll-a in turbid waters:
586 Validation. *Remote Sensing of Environment, 112*, 3582-3593
587 Gons, H.J. (1999). Optical teledetection of chlorophyll a in turbid inland waters. *Environ. Sci. Technol.,*
588 *33*, 1127-1132
589 Gons, H.J., Burger-Wiersma, T., Otten, J.H., & Rijkeboer, M. (1992). Coupling of phytoplankton and
590 detritus in a shallow, eutrophic lake (Lake Loosdrecht, The Netherlands). *Hydrobiologia, 233*, 51-59
591 Goodin, D.G., Han, L., Fraser, R.N., Rundquist, D.C., Stebbins, W.A., & Schalles, J.F. (1993). Analysis of
592 suspended solids in water using remotely sensed high resolution derivative spectra.
593 *Photogrammetric Engineering and Remote Sensing, 59*, 505–510
594 Gordon, H.R., Brown, O.B., Jacobs, M.M. (1975). Computed relationship between the inherent and
595 apparent optical properties of a flat homogeneous ocean. *Applied Optics*, 14, 417-427
596 Guanter, L., Ruiz-Verdu, A., Odermatt, D., FGiardino, C., Simis, S., Estelles, V., Heege, T.,
597 Dominguez-Gomez, J.A., & Moreno, J. (2010). Atmospheric correction of ENVISAT/MERIS data
598 over inland waters: Validation for European lakes. *Remote Sensing of Environment, 114*, 467-480
599 Hale, G.M., & Querry, M.R. (1973). Optical constants of water in the 200 nm to 200 micrometer
600 wavelength region. *Applied Optics, 12*, 555–563
601 Han, L., Rundquist, D.C., Liu, L.L., Fraser, R.N., & Schalles, J.F. (1994). The spectral responses of algal
602 chlorophyll in water with varying levels of suspended sediment. *International Journal of Remote*
603 *Sensing, 15*, 3707–3718
604 Hunter, P.D., Tyler, A.N., Presing, M., Kovacs, A.W., & Preston, T. (2008). Spectral discrimination of
605 phytoplankton colour groups: The effects of suspended particulate matter and sensor spectral
606 resolution. *Remote Sensing of Environment, 112*, 1527-1544
607 Khorram, S., Cheshire, H., Geraci, A., & Rosa, G. (1991). Water quality mapping of Augusta Bay, Italy
608 from Landsat TM data. *International Journal of Remote Sensing, 12*, 803-808
609 Kirk, J.T.O. (1994). *Light and Photosynthesis in Aquatic Ecosystem.* Cambridge, U.K.: Cambridge Univ.
610 Press
611 Kutser, T., Metsamaa, L., Strombeck, N., & Vahtmae, E. (2006). Monitoring cyanobacterial blooms by
612 satellite remote sensing. *Estuarine coastal and shelf science, 67*, 303-312
613 Kutser, T., Pierson, D.C., Kallio, K.Y., Reinart, A., & Sobek, S. (2005). Mapping lake CDOM by satellite
614 remote sensing. *Remote Sensing of Environment, 94*, 535-540
615 Le, C., Li, Y., Zha, Y., Sun, D., Huang, C., & Lu, H. (2009). A four-band semi-analytical model for
616 estimating chlorophyll a in highly turbid lakes: The case of Taihu Lake, China *Remote Sensing of*
617 *Environment, 113*, 1175-1182
618 Liu, Y., Islam, M.A., & Gao, J. (2003). Quantification of shallow water quality parameters by means of
619 remote sensing. *Progress in Physical Geography, 27*, 24-43
620 Mitchell, B.G. (1990). Algorithms for determining the absorption coefficient of aquatic particulates using

621 the quantitative filter technique (QFT). *Proc. SPIE, 1302*, 137
622 Mobley, C.D., Sundman, L.K., Davis, C.O., Bowles, J.H., Downes, T.V., Leathers, R.A., Montes, M.J.,
623 Bissett, W.P., Kohler, D.D.R., Reid, R.P., Louchard, E.M., & Gleason, A. (2005). Interpretation of
624 hyperspectral remote-sensing imagery by spectrum matching and look-up tables. *Applied Optics, 44*,
625 3576-3592
626 Morel, A. (1974). Optical properties of pure sea water. *Optical Aspects of Oceanography*. London, U.K.:
627 Academic
628 Morel, A., & Gentili, B. (1993). Diffuse reflectance of oceanic waters. II. Bidirectional aspects. *Applied*
629 *Optics, 32*, 6864-6879
630 Morel , A., & Gentili, B. (2009). A simple band ratio technique to quantify the colored dissolved and
631 detrital organic material from ocean color remotely sensed data. *Remote Sensing of Environment, 113*,
632 998-1011
633 Morel , A., & Prieur, L. (1977). Analysis of variations in ocean color. *Limnology and Oceanography, 22*,
634 709-722
635 Mueller, J.L., Davis, C., Arnone, R., Frouin, R., Carder, K., & Lee, Z.P. (2000). Above-water radiance and
636 remote sensing reflectance measurements and analysis protocols. *Ocean Optics protocols for*
637 *satellite ocean color sensor validation Revision 2* (pp. 98-107). Greenbelt, Maryland: National
638 Aeronautical and Space Administration
639 Nichol, J.E. (1993). Remote sensing of water quality in the Singapole–Johor–Riau growth triangle.
640 *Remote Sensing of Environment, 43*, 139-148
641 Novo, E.M.L.M., Barbosa, C.C.F., Freitas, R.M., Shimabukuro, Y.E., Melack, J.M., & Filho, W.P. (2006).
642 Seasonal change in chlorophyll distributions in Amazon floodplain lakes derived from MODIS
643 images. *Limnology, 7*, 153-161
644 Oyama, Y., Matsushita, B., Fukushima, T., Matsushige, K., & Imai, A. (2009). Application of spectral
645 decomposition algorithm for mapping water quality in a turbid lake (Lake Kasumigaura, Japan)
646 from Landsat TM data. *ISPRS Journal of Photogrammetry & Remote Sensing, 64*, 73-85
647 Oyama, Y., Matsushita, B., Fukushima, T., Nagai, T., & Imai, A. (2007). A new algorithm for estimating
648 chlorophyll-a concentration from multi-spectral satellite data in Case II waters: A simulation based
649 on a controlled laboratory experiment. *International Journal of Remote Sensing, 28*, 1437-1453
650 Pope, R.M., & Fry, E.S. (1997). Absorption spectrum (380–700 nm) of pure water. II. Integrating cavity
651 measurements. *Applied Optics, 36*, 8710
652 Santini, F., Alberotanza, L., Cavalli, R.M., & Pignatti, S. (2010). A two-step optimization procedure for
653 assessing water constituent concentrations by hyperspectral remote sensing techniques: An
654 application to the highly turbid Venice lagoon waters. *Remote Sensing of Environment, 114*, 887-898
655 SCOR-UNESCO (1966). Determination of photosynthetic pigment in seawater. Monographs on
656 oceanographic methodology. In. Paris, France
657 Svab, E., Tyler, A.N., Perston, T., Presing, M., & Balogh, K.V. (2005). Characterizing the spectral
658 reflectance of algar in lake waters with high suspended sediment concentrations. *International*
659 *Journal of Remote Sensing, 26*, 919-928
660 Tyler, A.N., Svab, E., Preston, T., Présing, M., & Kovács, W.A. (2006). Remote sensing of the water
661 quality of shallow lakes: A mixture modeling approach to quantifying phytoplankton in water
662 characterized by high-suspended sediment. *International Journal of Remote Sensing, 27*, 1521-1537

Van Der Woerd, H.J., & Pasterkamp, R. (2008). HYDROPT: A fast and flexible method to retrieve chlorophyll-a from multispectral satellite observations of optically complex coastal waters. *Remote Sensing of Environment, 112*, 1795-1807

Yang, W., Matsushita, B., Chen, J., Fukushima, T., & Ma, R. (2010). An Enhanced Three-Band Index for Estimating Chlorophyll-a in Turbid Case-II Waters:Case Studies of Lake Kasumigaura, Japan, and Lake Dianchi, China. *IEEE Geoscience and Remote Sensing Letters*, in press

Zhang, Y., Liu, M., Qin, B., Woerd, H.J., Li, J., & Li, Y. (2009). Modeling Remote-Sensing Reflectance and Retreving Chlorohpyll-a Concentration in Extremely Turbid Case-2 Waters (Lake Taihu, China). *IEEE Transactions on Geoscience and Remote Sensing, 47*, 1937-1948

List of Tables

Table 1. Spectral characteristics of the Medium Resolution Imaging Spectrometer (MERIS)

Band	Band Centre (nm)	Bandwidth (nm)	Spatial Resolution (m)	Swath Width	Quantization
1	412.5	10	300	1150 km	12 bits
2	442.5	10	300		
3	490	10	300		
4	510	10	300		
5	560	10	300		
6	620	10	300		
7	665	10	300		
8	681.25	7.5	300		
9	708.75	10	300		
10	753.75	7.5	300		
11	761.75	3.75	300		
12	778.75	15	300		
13	865	20	300		
14	885	10	300		
15	900	10	300		

Table 2 Demonstration of a look-up table (LUT) for the [Chl-a]-estimation models, where [TR] and [CDOM] have units of g m^{-3} and m^{-1}, respectively

[CDOM] \ [TR]	1	2	…	…	249	250
0.1	$(p_{1,1}; q_{1,1}; r_{1,1})$	$(p_{1,2}; q_{1,2}; r_{1,2})$	…	…	$(p_{1,249}; q_{1,249}; r_{1,249})$	$(p_{1,250}; q_{1,250}; r_{1,250})$
0.2	$(p_{2,1}; q_{2,1}; r_{2,1})$	$(p_{2,2}; q_{2,2}; r_{2,2})$	…	…	$(p_{2,249}; q_{2,249}; r_{2,249})$	$(p_{2,250}; q_{2,250}; r_{2,250})$
0.3	$(p_{3,1}; q_{3,1}; r_{3,1})$	$(p_{3,2}; q_{3,2}; r_{3,2})$	…	…	$(p_{3,249}; q_{3,249}; r_{3,249})$	$(p_{3,250}; q_{3,250}; r_{3,250})$
…	…	…	…	…	…	…
…	…	…	…	…	…	…
9.9	$(p_{99,1}; q_{99,1}; r_{99,1})$	$(p_{99,2}; q_{99,2}; r_{99,2})$	…	…	$(p_{99,249}; q_{99,249}; r_{99,249})$	$(p_{99,250}; q_{99,250}; r_{99,250})$
10	$(p_{100,1}; q_{100,1}; r_{100,1})$	$(p_{100,2}; q_{100,2}; r_{100,2})$	…	…	$(p_{100,249}; q_{100,249}; r_{100,249})$	$(p_{100,250}; q_{100,250}; r_{100,250})$

Table 3. Accuracy assessment of the SAMO-LUT and previous semi-analytical algorithms using noise-free simulation data, *in situ* collected data and MERIS data

	Simulation data		***In situ* data**		**MERIS data**	
	SAMO-LUT	Semi-analytical Algorithms (Eq. 13-15)	SAMO-LUT	Semi-analytical Algorithms (Eq. 13-15)	SAMO-LUT	Semi-analytical Algorithms (Eq. 13-15)
[Chl-a]						
RMSE (mg m^{-3})	0.43	45.83	3.37	3.60	12.64	28.54
MNB (%)	-0.06	15.26	-1.58	-1.77	7.58	23.82
NRMS (%)	2.41	328.84	3.65	4.06	16.81	34.34
R^2	1.00	0.83	0.98	0.90	0.76	0.31
[TR]						
RMSE (g m^{-3})	0.42	16.07	1.81	8.50	4.44	11.53
MNB (%)	1.74	48.64	3.83	-4.49	-2.85	45.97
NRMS (%)	2.26	359.69	6.73	35.87	23.32	106.26
R^2	1.00	0.96	0.89	0.14	0.89	0.32
[CDOM]						
RMSE (m^{-1})	0.06	3.36	0.21	1.42	0.32	1.11
MNB (%)	-0.62	139.62	-7.07	388.64	8.74	115.07
NRMS (%)	8.12	1160.92	31.19	375.26	33.62	130.57
R^2	0.99	0.04	0.78	0.26	0.26	0.02

List of Figures

Fig. 1. Distribution of sampling sites in (A) Lake Dianchi, China and (B) Lake Kasumigaura, Japan; and four corresponding MERIS images. (The red stars, green squares and blue circles in (A) denote sampling sites for Lake Dianchi in Oct. 2007, Mar. 2009 and Jul. 2009, respectively; the red circles and green circles in (B) denote sampling sites in Lake Kasumigaura for Feb. 2006 and Aug. 2008, respectively.)

Fig. 2. Specific inherent optical properties (SIOPs) of Lake Dianchi. (A): a_{ph}^* [m^2 mg^{-1}], a_{tr}^* [m^2 g^{-1}], and a_{CDOM}^* [dimensionless] are specific absorption coefficients of phytoplankton, tripton, and colored dissolved organic matter, respectively; a_w [m^{-1}] is the absorption coefficient of pure water. (B): $b_{b,ph}^*$ [$m^2 mg^{-1}$] and $b_{b,tr}^*$ [$m^2 g^{-1}$] are the specific backscattering coefficients of phytoplankton and tripton, respectively; and $b_{b,w}$ [m^{-1}] is the backscattering coefficient of pure water.

Fig. 3. Comparison of modeled remote-sensing reflectance spectra just above the water surface and measured spectra.

Fig. 4. Initial estimation models for (A) chlorophyll *a* concentration; (B) tripton concentration; and (C) CDOM absorption at 440 nm based on previous semi-analytical indices.

715 Fig. 5. Examples of estimation models for (A) chlorophyll *a* concentration when tripton
716 concentration and CDOM absorption at 440 nm are constants; (B) tripton concentration when
717 chlorophyll *a* concentration and CDOM absorption at 440 nm are constants; (C) CDOM absorption
718 at 440 nm when chlorophyll *a* concentration and tripton concentration are constants.
719
720 Fig. 6. Flowchart of the SAMO-LUT method.
721
722 Fig. 7. Comparison of true and estimated (A) [Chl-a]; (B) [TR]; and (C) [CDOM] for a noise-free
723 simulation dataset.
724
725 Fig. 8. Comparison of measured and estimated (A) [Chl-a]; (B) [TR]; and (C) [CDOM] for an *in situ*
726 collected dataset in Lake Dianchi.
727
728 Fig. 9. Comparison between *in situ* collected and atmospheric corrected remote-sensing reflectance
729 spectra in Lake Dianchi. (A)-(C) are for three sampling sites on Oct. 24, 2007, and (D)-(F) are for
730 three sampling sites with lower latitudes on Mar. 13, 2009 (See Fig. 1A).
731
732 Fig. 10. Comparison of measured and estimated (A) [Chl-a]; (B) [TR]; and (C) [CDOM] for MERIS
733 data in Lake Dianchi and Lake Kasumigaura during four periods.
734
735
736
737
738
739
740
741
742
743
744
745
746
747
748
749
750

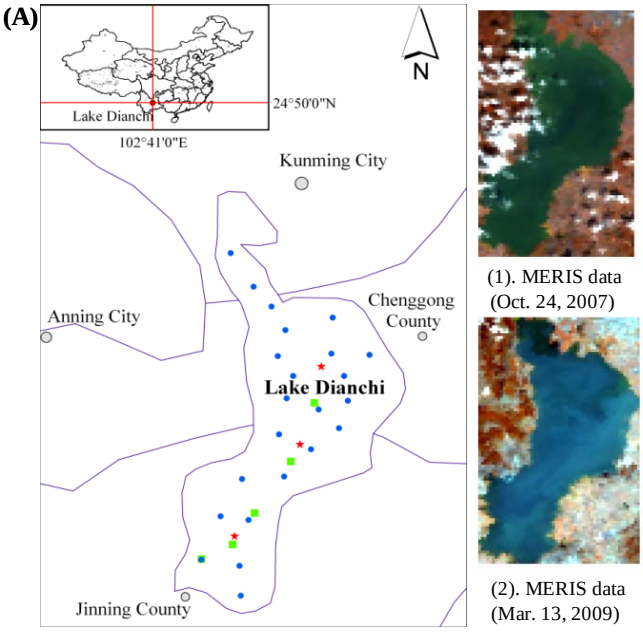

751

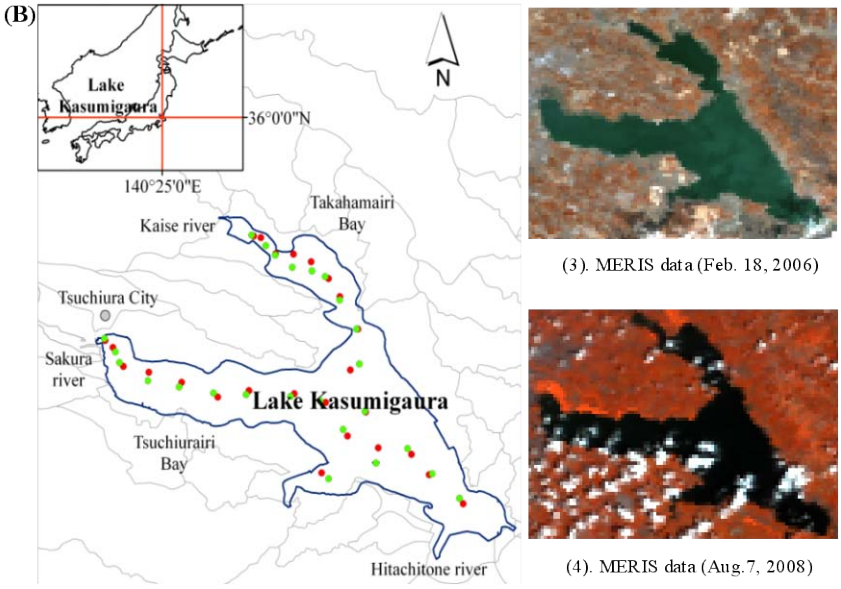

752

753 Fig. 1.

754

755

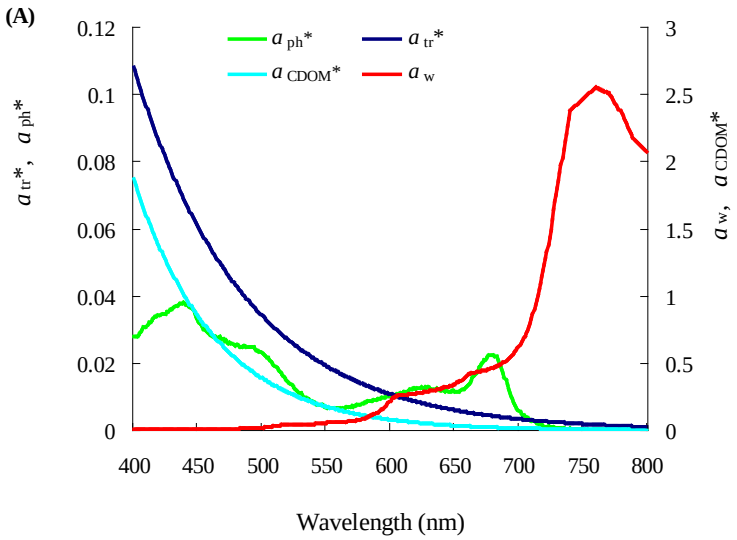

756

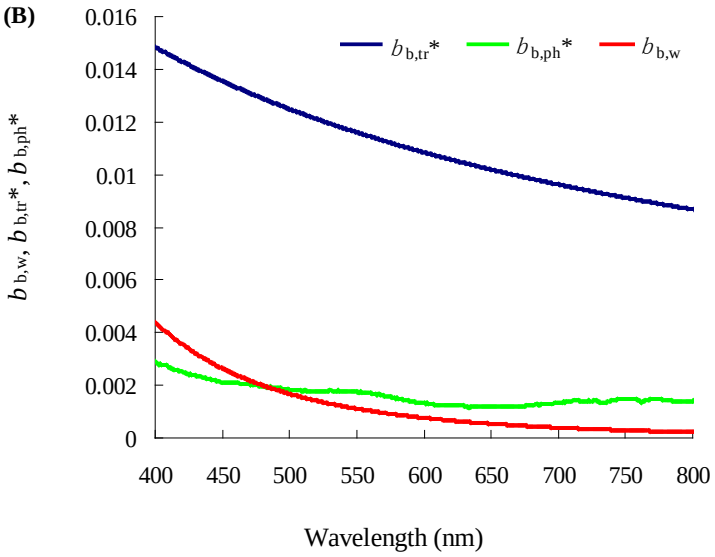

757

758 Fig. 2.

759

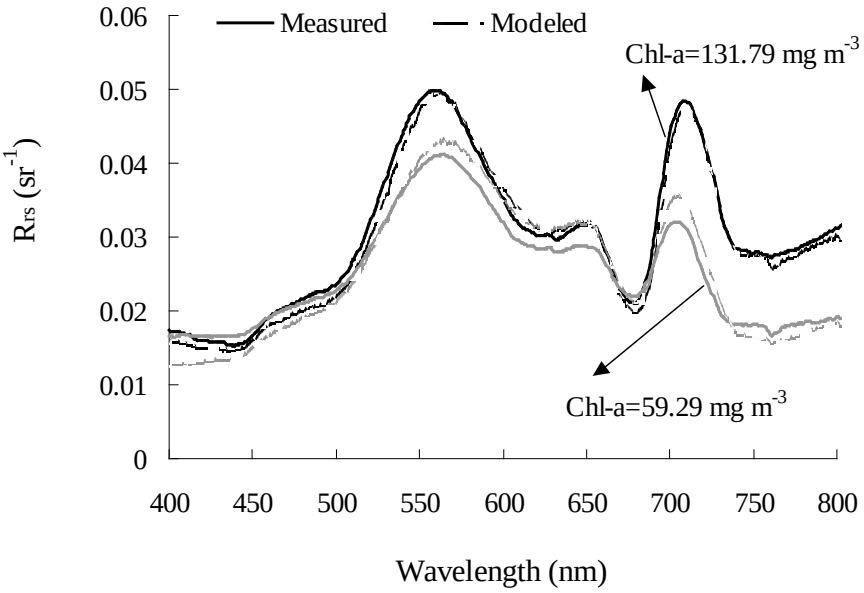

760

761 Fig. 3.

762

763

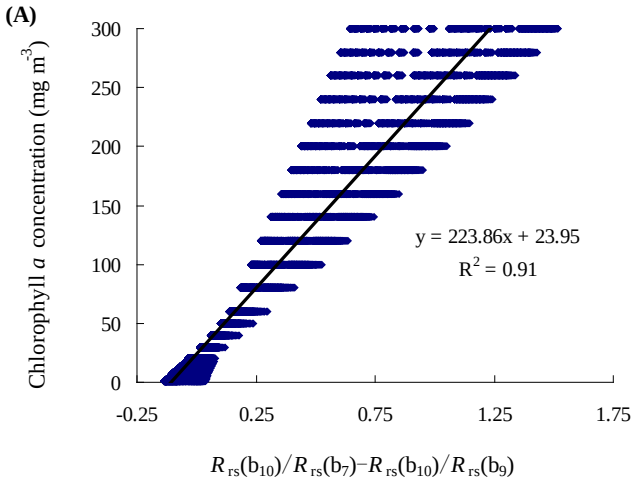

764

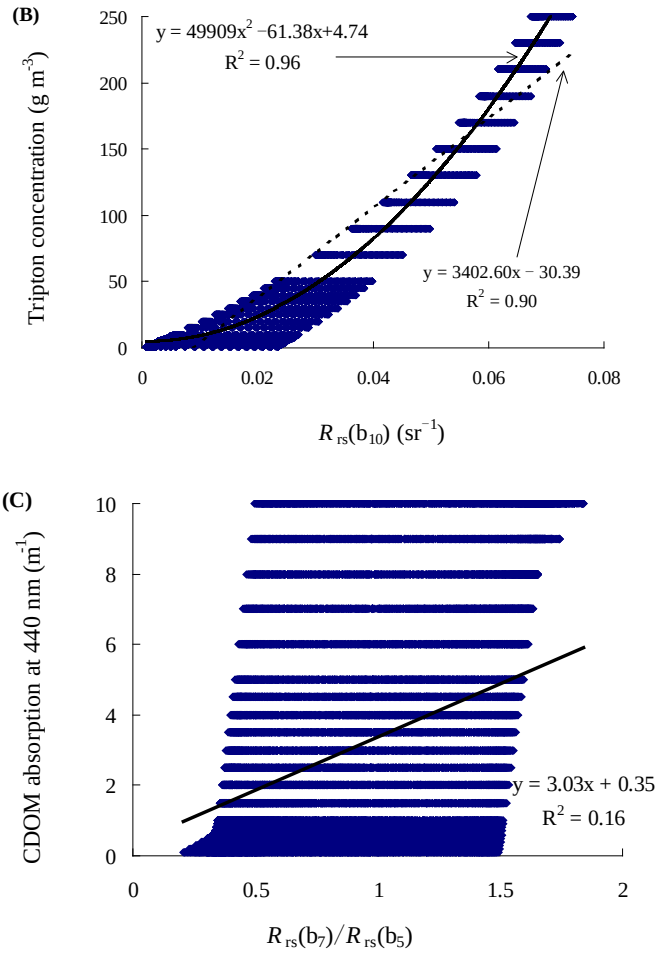

765

766

767 Fig. 4.

768

769

770

771

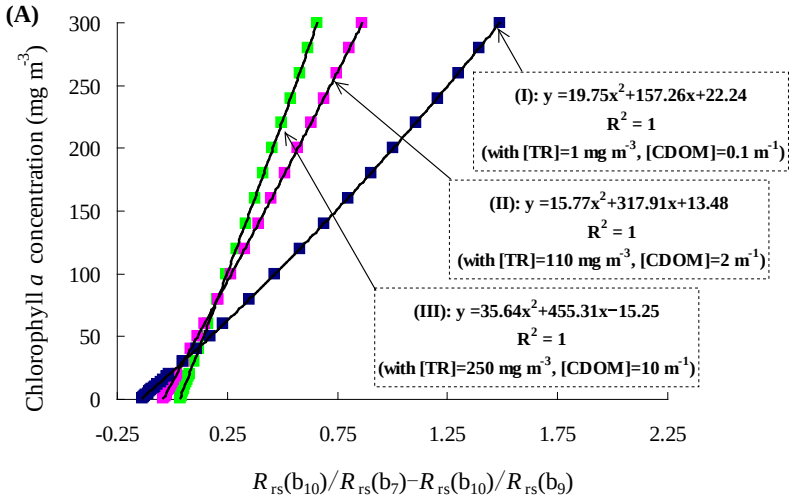

772

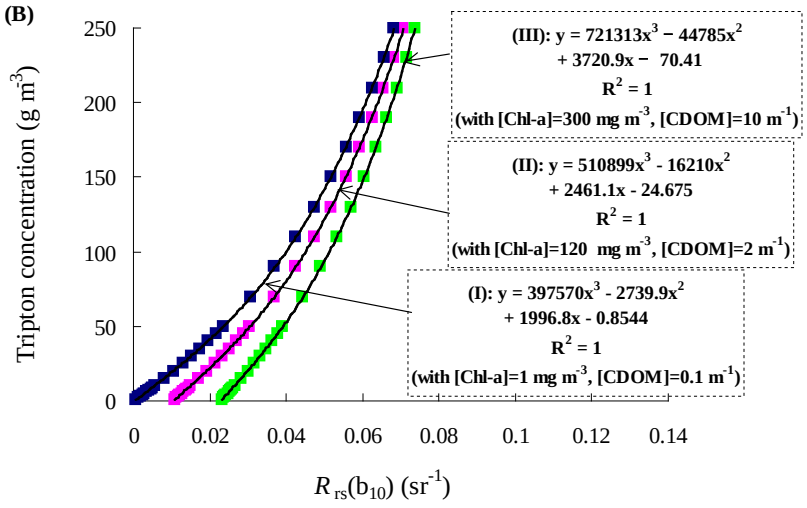

773

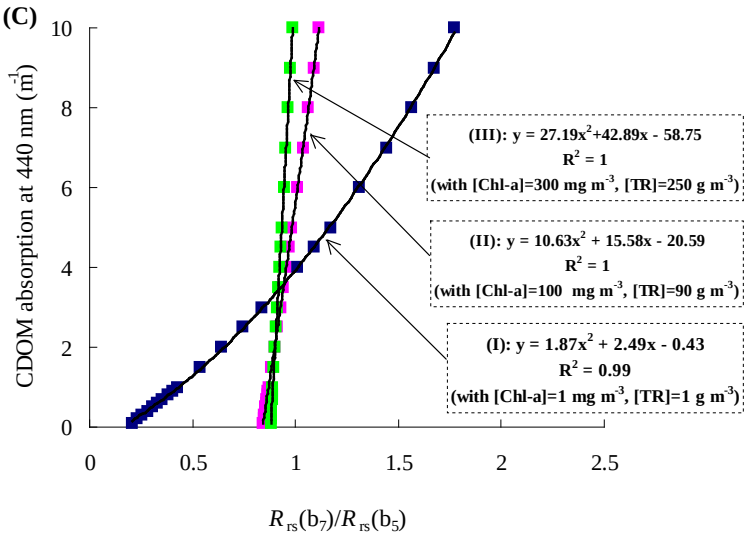

774

775 Fig. 5.

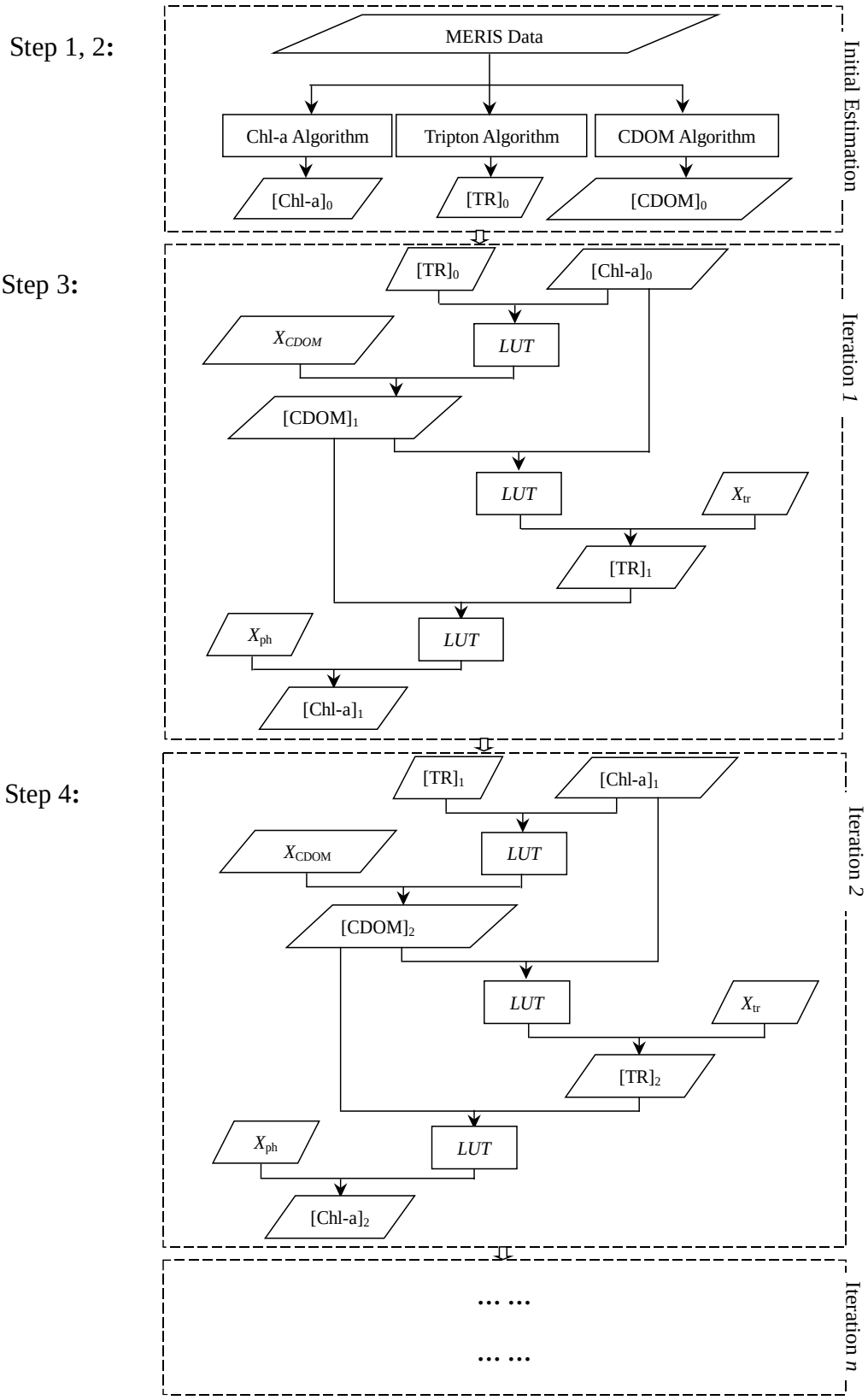
Step 1, 2:
Step 3:
Step 4:
MERIS Data
Chl-a Algorithm
Tripton Algorithm
CDOM Algorithm
[Chl-a]0
[TR]0
[CDOM]0
Initial Estimation
[TR]0
[Chl-a]0
XCDOM
LUT
[CDOM]1
LUT
Xtr
[TR]1
Xph
LUT
[Chl-a]1
Iteration 1
[TR]1
[Chl-a]1
XCDOM
LUT
[CDOM]2
LUT
Xtr
[TR]2
Xph
LUT
[Chl-a]2
Iteration 2
… …
… …
Iteration n

Fig. 6.

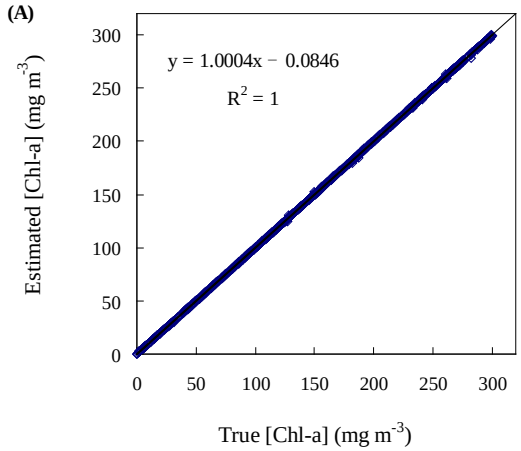

778

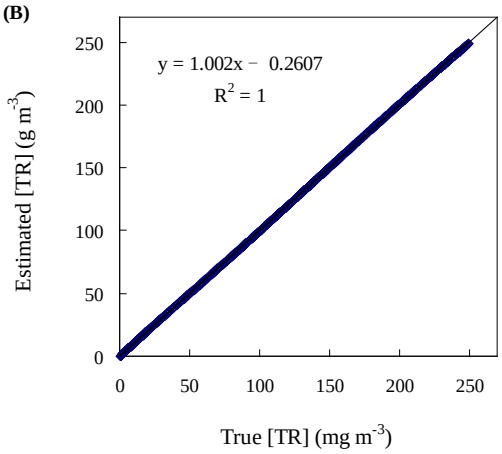

779

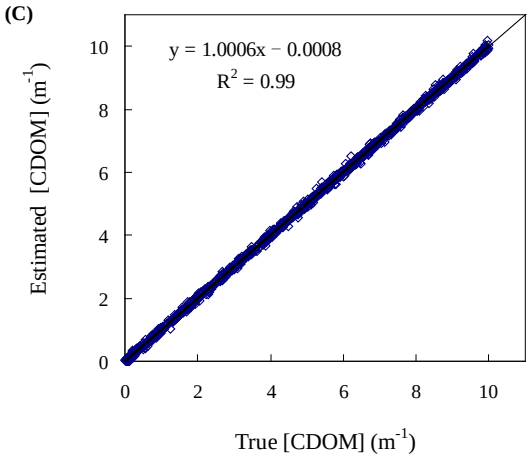

780

781 Fig. 7.

782

783

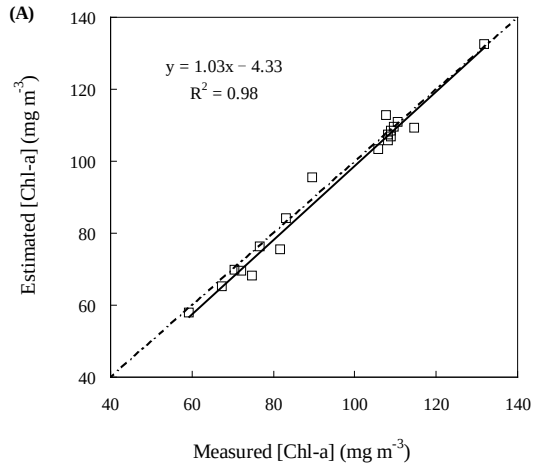

784

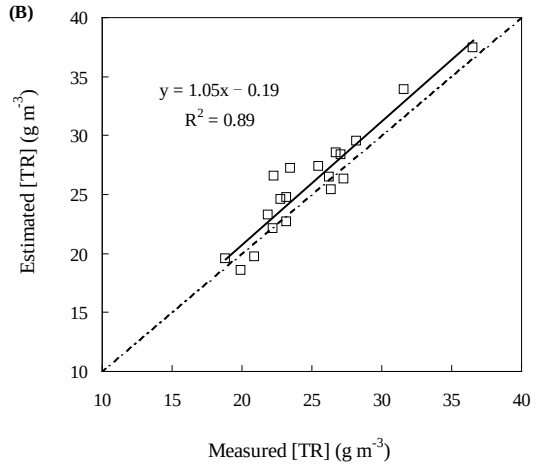

785

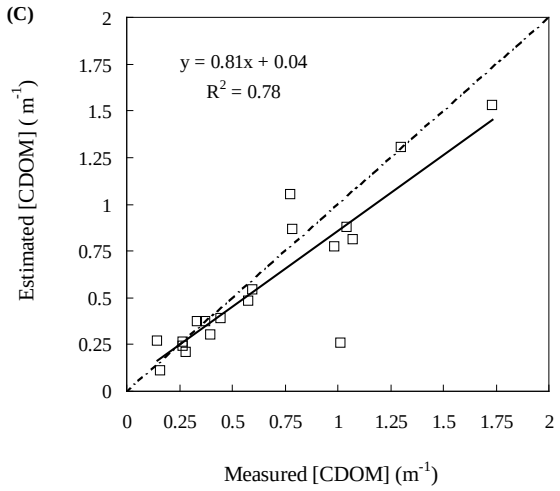

786

787 Fig. 8.

788

789

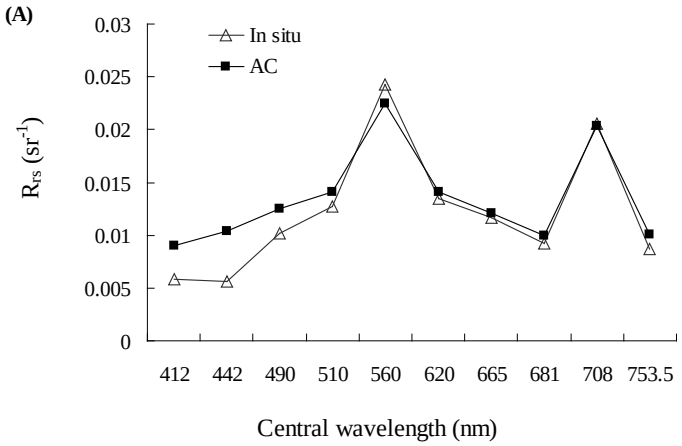

790

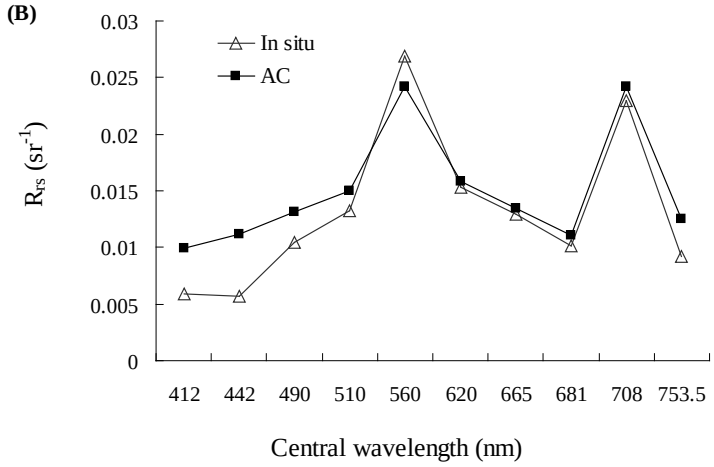

791

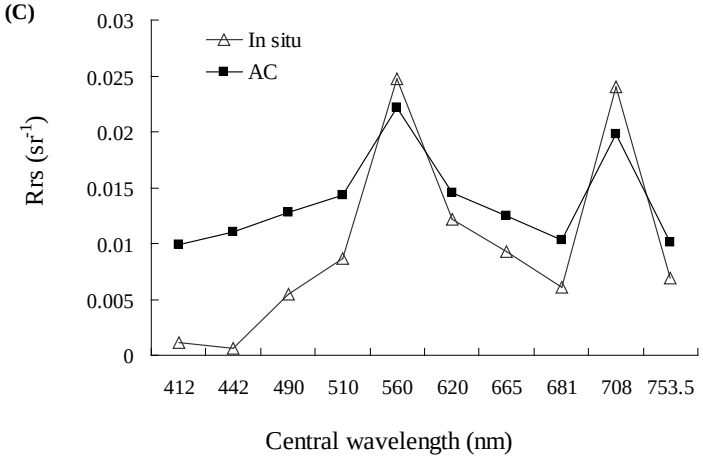

792

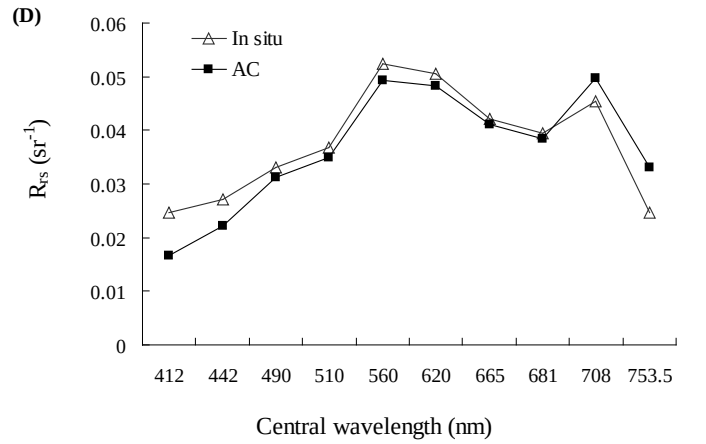

793

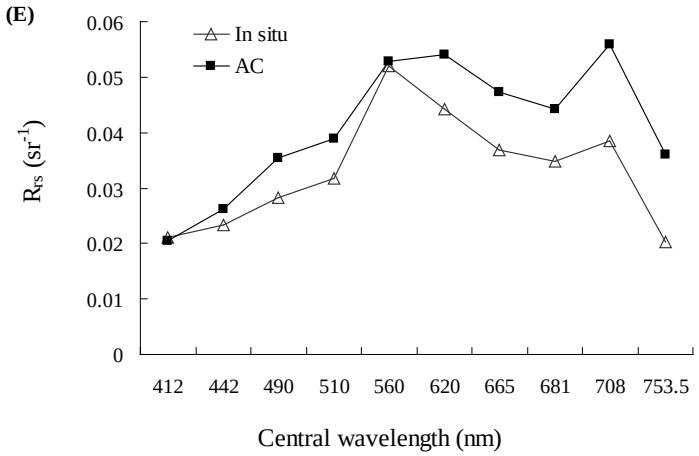

794

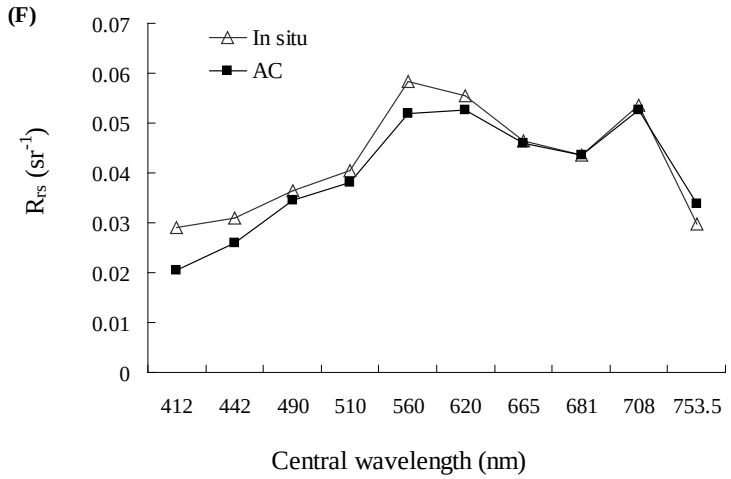

795

796 Fig. 9.

797

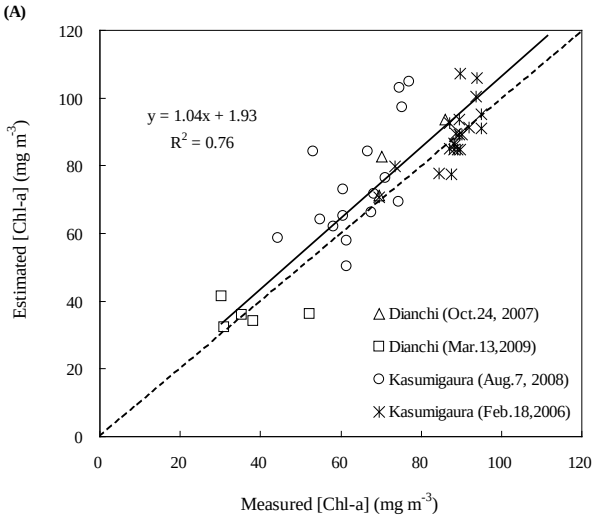

798

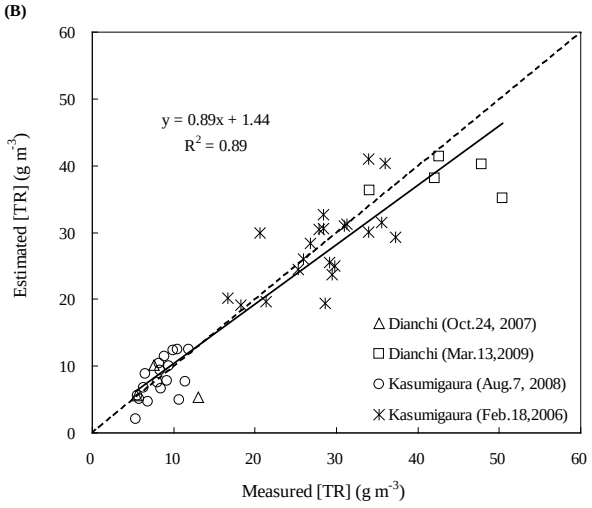

799

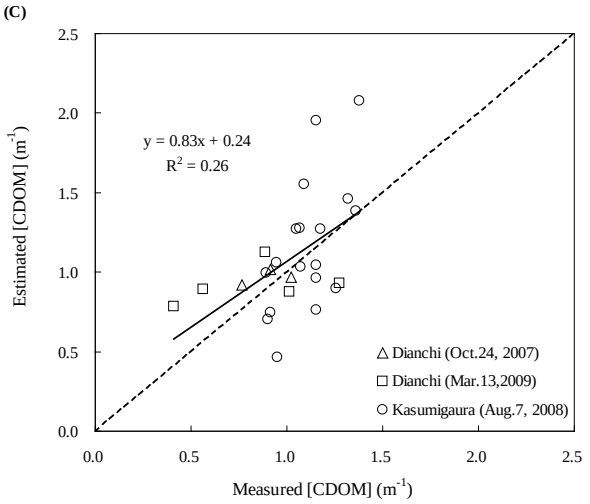

800

801 Fig. 10.

802